LIMNOLOGY
and
OCEANOGRAPHY: METHODS

ASLO

*Limnol. Oceanogr.: Methods* 00, 2017, 00–00

doi: 10.1002/lom3.10218

# Analyzing the shape of observed trait distributions enables a data-based moment closure of aggregate models

**Ursula Gaedke, * Toni Klauschies**
Department of Ecology - Ecosystem modelling, Potsdam University, Potsdam, Germany

## *Abstract*

The shape of trait distributions may inform about the selective forces that structure ecological communities. Here, we present a new moment-based approach to classify the shape of observed biomass-weighted trait distributions into normal, peaked, skewed, or bimodal that facilitates spatio-temporal and cross-system comparisons. Our observed phytoplankton trait distributions exhibited substantial variance and were mostly skewed or bimodal rather than normal. Additionally, mean, variance, skewness und kurtosis were strongly correlated. This is in conflict with trait-based aggregate models that often assume normally distributed trait values and small variances. Given these discrepancies between our data and general model assumptions we used the observed trait distributions to test how well different aggregate models with first- or second-order approximations and different types of moment closure predict the biomass, mean trait, and trait variance dynamics using weakly or moderately nonlinear fitness functions. For weakly non-linear fitness functions aggregate models with a second-order approximation and a data-based moment closure that relied on the observed correlations between skewness and mean, and kurtosis and variance predicted biomass and often also mean trait changes fairly well and better than models with first-order approximations or a normal-based moment closure. In contrast, none of the models reflected the changes of the trait variances reliably. Aggregate model performance was often also poor for moderately nonlinear fitness functions. This questions a general applicability of the normal-based approach, in particular for predicting variance dynamics determining the speed of trait changes and maintenance of biodiversity. We evaluate in detail how and why better approximations can be obtained.

Trait-based ecology greatly contributes to a detailed understanding of population and community dynamics (Norberg 2004). Functional traits are used to link species to their functions in the ecosystem (McGill et al. 2006; Hillebrand and Matthiessen 2009; Enquist et al. 2015). They are well-defined, measureable properties of species (e.g., body size, edibility, or diet selectivity) affecting their performance, trophic interactions and responses to environmental changes and hence community dynamics. The standing variation of an individual trait, i.e., the presence and abundance of different trait values within a community at a given moment in time, can be represented by a single continuous trait distribution. The latter can be described by its central moments: The mean indicates the trait value of the most abundant species when the trait distribution is unimodal and fairly symmetric. The variance denotes the functional diversity present within a community. The symmetry and peakedness of a trait distribution can be further estimated from its skewness and kurtosis.

The mean, variance and shape of a trait distribution may change in response to selection and inform in a concise and comparable way about the dominant trait values, the actual trait range (functional diversity) and the type of prevailing selection pressure (e.g., stabilizing or disruptive). This implies a demand to describe systematically the shape of trait distributions enabling spatio-temporal and cross-system comparisons. Using standard statistical tests for this purpose often fails because the number of observations is typically unknown for plankton samples or changes pronouncedly along the trait axis. Therefore, we developed a method that enables the classification of the shape of trait distributions into normal, peaked, skewed, or bimodal solely based on the first four central moments (mean, variance, skewness, and kurtosis) of the trait distribution. These measures are obtained easily and reliably from plankton observations and it is not required to define a priori a distribution to which the data are fitted or tested against.

*Correspondence: gaedke@uni-potsdam.de

Additional Supporting Information may be found in the online version of this article.

U.G. and T.K. have contributed equally to this work.

Knowledge on the shape of trait distributions is also essential when using trait-based aggregate models. Full trait distribution models that account for all possible trait values can describe the dynamics of the mean, variance and shape of trait distributions most accurately (Coutinho et al. 2016). However, their rather high complexity may require long simulation times and may prevent a general understanding of the model behavior. Thus, ecologists recently advocated trait-based aggregate models (also called dynamic trait or gradient dynamics models) to keep model complexity low and facilitate insights into the mechanisms underlying changes in the community composition. Their equations inform directly about the properties of the fitness landscape and trait distribution that drive the temporal dynamics of the summed biomasses, mean trait values, and trait variances (Wirtz and Eckhardt 1996; Merico et al. 2009). Thus, the strong reduction in the system's dimensionality promotes rigorous analytic considerations and computational efficiency. Such models have been used successfully to better understand principal patterns in idealized or natural communities, including eco-evolutionary dynamics and biomass-trait feedbacks. For example, they were used to study the mutual adjustments of traits in predator and prey communities and their consequences for community dynamics (Tirok et al. 2011) and biogeographical differences in the size composition of phytoplankton communities (Acevedo-Trejos et al. 2015) (for other applications see below). When tailored to specific systems either entire communities were considered (Merico et al. 2009; Wirtz and Sommer 2013; Smith et al. 2016) or functional groups covering more restricted trait ranges (Norberg et al. 2001; Terseleer et al. 2014).

The appealingly low number of state variables and thus reduction in model complexity is achieved at the cost of making simplifying assumptions about the shape of the trait distribution and the curvature of the relationship between trait values and per capita net growth rates, i.e., the fitness function. Inevitably, this reduces the accuracy of the model results. Here, we evaluate under which conditions major inaccuracies are to be expected and how they can be reduced. In line with the approach of quantitative genetics (Lande 1976, 1982) community ecologists often assumed the trait distributions to be normal and to exhibit small variances and a constant shape. This facilitates to approximate the trait distributions by up to their first four central moments and to resolve the fitness functions only locally around the mean trait value. However, in contrast to the distribution of quantitative traits at the population level where some inherent justification for the assumption of normality exists and its limitations are rather well understood (e.g., Lande 1976; Abrams et al. 1993; Turelli and Barton 1994) there is no clear reason or strong empirical evidence that trait values are generally normally distributed at the community level. A thoroughly testing for normality and the consequences of potential deviations is still lacking.

Thus, the second objective of this study is to evaluate to what extent aggregate models can adequately represent the changes of the biomasses, mean trait values and trait variances in real ecosystems. This implies evaluating (1) the variance and shape of trait distributions observed in natural ecosystems using the abovementioned classification method, and (2) the deviations arising between full and aggregate models due to the approximations made.

We put the first issue into practice using comprehensive observations of the distributions of two traits in phytoplankton communities from two different habitats. Phytoplankton communities provide an ideal testing ground for this purpose. They contribute about half of the global primary production and their dynamics have often been modeled using trait-based approaches (Wirtz and Eckardt 1996; Merico et al. 2009; Kremer and Klausmeier 2013; Terseleer et al. 2014). Furthermore, they typically undergo pronounced changes in response to abiotic and biotic forcing that may lead to a large range of differently shaped trait distributions. We use high frequency long-term measurements in two temperate freshwater bodies differing in their physico-chemical properties and algal growth conditions, large deep Lake Constance (1979–1999, 853 sampling dates) and small Saidenbach Reservoir (1975–2002, 1259 sampling dates). Generalizing our findings, we consider two different traits, cell size (i.e., volume) and maximum length. They are closely related to the usually most influential processes in phytoplankton dynamics, growth and grazing losses. We test the validity of the aggregate model assumptions by evaluating the magnitude of the trait variance, the relative share of normal-like, peaked, skewed, and bimodal trait distributions and correlations among lower and higher moments.

Subsequently, we use the observed trait distributions to test how well the results of different aggregate models fit with the ones of a corresponding full model. This depends on the type of aggregate model and fitness function employed. The fitness function may have a complex shape and is model specific as it depends typically in a non-linear way on the different factors influencing net growth (e.g., light, nutrients, grazing, and sedimentation for phytoplankton). To achieve nevertheless generalizable results, we combine four types of aggregate models of increasing complexity with two common types of non-linearities with high ecological relevance representing our fitness functions. We consider a weak non-linearity represented by an allometric relationship between growth rates and cell volume, and a moderately non-linear, logistic fitness function. The latter reflects a rather smooth transition along the trait gradient (here maximum cell length) from high to low values such as the feeding rate on edible and less edible prey. The outcome of the aggregate models is compared to a full model accounting for the entire fitness landscape and the full shape of the trait distribution observed at a distinct sampling date (i.e., we do not aim to estimate potential long-term changes in the trait distribution due to selection pressure imposed by the fitness function).

The reduction in complexity achieved by aggregate models restricts resolving potentially non-linear fitness functions only locally around the current mean trait value and approximating the exact shape of the trait distribution by the first moments (Coutinho et al. 2016). Different types of aggregate models exist along a gradient of increasing complexity and precision depending on the accuracy of approximation and moment closure involved. Models using a first order-approximation consider only temporal changes in the total biomasses and mean trait values, whereas second-order approximations account also for the temporal changes in the trait variance. A first-order approximation implies that changes in the mean trait value are only based on the local fitness gradient, i.e., the first derivative of the fitness function evaluated at the mean trait value. Furthermore, the trait variance is either kept constant in time or estimated from the mean trait value. Hence, reliable results can generally be expected for rather linear fitness functions or small standing trait variation so that the trait distributions at a given time or location are well represented by their mean (Bolnick et al. 2011). It remains, however, to be tested whether these conditions prevail in natural systems.

Second-order approximations account additionally for the second derivative of the fitness function. This enables them to capture to some degree also non-linearities in the fitness function. Furthermore, they usually account for the variance and its dynamics and resolve the shape of the trait distributions to a higher degree by considering also the skewness and kurtosis. The latter can be achieved by assuming a particular shape of the trait distribution, e.g., normal, or by using data-based relationships between skewness and mean, and kurtosis and variance. Thus, aggregate models based on such a second-order approximation are expected to perform well for weakly non-linear fitness functions combined with rather normal trait distributions, or trait distributions with distinct correlations between the lower and higher moments enabling a data-based moment closure. Small standing variances will also improve the accuracy of the predictions (Wirtz and Eckhardt 1996; Norberg et al. 2001; Tirok et al. 2011; Coutinho et al. 2016).

Using our novel and robust tool to classify the shape of trait distributions into four common types, we show that non-normal phytoplankton trait distributions with substantial variance are the rule rather than the exception. We found a high prevalence of skewness and multi- or bimodality for both traits and both habitats and pronounced temporal changes in the shape of trait distributions. Hence, aggregate models assuming normal trait distributions likely deliver inaccurate results. For a weakly non-linear fitness function, the arising errors could be counteracted best using second-order approximations with a data-based moment closure. They yielded reliable predictions for the temporal biomass changes and partly also the trait changes but changes in the variance were prone to substantial errors. For moderately non-linear fitness functions, the reliability of aggregate models has to be severely questioned and we suggest a combination with species sorting models (Tirok and Gaedke 2010) to reduce the variances of the individual trait distributions and the non-linearities of the individual fitness functions (Klauschies et al. 2016). Our results and conclusions may also apply to other fields as aggregate approaches were also used in e.g., spatial ecological (Gandhi et al. 2000) and social-economical models (Wirtz and Lemmen 2003) and fishery management (Akpalu 2009).

## Materials and procedures

### Data acquisition

Upper Lake Constance (LC, German: Bodensee) is a large (472 $km^2$), deep (mean depth = 101 m), warm-monomictic temperate lake north of the European Alps. During the study period 1979–1999 it underwent re-oligotrophication and mean annual phytoplankton biomass declined by a factor of 2 (Gaedke 1998). This indicates that the long-term changes are small compared to the very pronounced seasonal dynamics as individual species vary in density by a factor of 10–1000 or more during the year and total biomass by a factor of more than 20 (Rocha et al. 2011*a*). Culminating in 853 sampling dates between 1979 and 1999, the sampling was conducted weekly during the growing season and approximately fortnightly in winter (for details *see* Gaedke 1998). We aggregated the numerous species encountered into 36 morphotypes comprising individual species or higher taxonomic units that have identical or very similar trait values and contributed to more than 92% of the total phytoplankton biomass (cf. Rocha et al. 2011*b*; Weithoff et al. 2015). The average number of morphotypes encountered per sampling date amounts to $17 \pm 6$.

Saidenbach Reservoir (SR) is a small dimictic drinking water reservoir (area 1.5 $km^2$, volume $22 \times 10^6$ $m^3$) with an average and maximum depth of about 15 m and 45 m, respectively, situated in the low mountain range of southern East Germany (Horn et al. 2011). Its trophic state changed from mesotrophic to eutrophic in the 1970s, remained eutrophic in the 1980s and quickly returned to the mesotrophic state due to a strong reduction of the phosphorous import since 1990 after German Reunification. Supported by the Saxony Academy of Science and hosted at the Ecological Station Neunzehnhain of the Technical University of Dresden, Heidemarie Horn analyzed the phytoplankton weekly from 1975 to 1985 and fortnightly until 2011, culminating in 1259 sampling dates (for details *see* Horn 2003; Horn et al. 2011, 2015). As in LC, samples were counted with an inverted microscope. The average number of morphotypes encountered per sampling date was $25 \pm 16$.

### Selection of traits

We selected two regularly measured traits, cell volume (expressed in $\mu m^3$/cell), and maximum length, (i.e., longest

linear dimension, measured in $\mu$m) which are of outstanding importance for the fitness of phytoplankton species (Weithoff 2003; Litchman et al. 2007; Horn et al. 2011) and clearly related to the observed phytoplankton biomass dynamics in LC (Tirok and Gaedke 2007; Vasseur and Gaedke 2007; Rocha et al. 2012). According to allometric theory, cell volume influences many physiological activities such as nutrient uptake and maximum growth rates. The classification was done according to the individual cell volume of single-celled and colony-forming morphotypes. In addition, the shape of a cell or colony is important with respect to their ability to absorb nutrients, susceptibility to sedimentation and to filter-feeding zooplankton grazing. A suitable measure for these processes is the maximum length (i.e., the longest linear dimension) for which the classification was done according to the individual cell size, filament length or colony size. The two traits cell volume and maximum length were only moderately correlated (log (size) vs. log (length) $r^2 = 0.58$ for LC and $r^2 = 0.30$ for SR) due to the frequently elongated or complex shape of in particular the larger phytoplankton cells.

We $\log_2$-transformed both trait values to account for their large range (covering over 4 and 3 orders of magnitude, respectively) and for the inherent skewness in size distributions (Terseleer et al. 2014; Acevedo-Trejos et al. 2015). For ease of comparison, we grouped the biomass of the morphotypes into 19 (cell volume) or 35 (maximum length) equidistant classes on a $\log_2$ scale. To account for individual growth and variability within each morphotype, we assumed that the minimum and the maximum trait values of each morphotypes differ by a factor of $a = 4$ for cell volume and $a = 2$ for length prior to $\log_2$-transformation (Gaedke 1992). Following the shape of a normal distribution, we allocated 50% of the biomass to the class corresponding to the mean trait value, $\bar{x}$, 20% to the two adjacent classes corresponding to the $a^{1/4}$ and $a^{-1/4}$ of $\bar{x}$ and 5% to the classes corresponding to the $a^{1/2}$ and $a^{-1/2}$ of $\bar{x}$. All subsequent calculations are based on the mean trait values of the classes. For a relative comparison between the two traits, we standardized their variances by dividing them by their theoretical maximum values (45 for size and 18 for length). The maximum variance was obtained by allocating 50% of the biomass to each of the most extreme trait values possible.

**Characterizing trait distributions based on their shape**

Our classification scheme categorizes trait distributions based on their dominant shape properties which are directly related to their first four standardized central moments: mean, $\bar{x}$, standing variance, $v$, skewness, $S$, and kurtosis, $K$. They are calculated for both traits and each sampling date after Eqs. 1–4:

$$\bar{x} = \sum_{i=1}^{N} w_i \cdot x_i \tag{1}$$

$$v = \sum_{i=1}^{N} w_i \cdot (x_i - \bar{x})^2 \tag{2}$$

$$S = \sum_{i=1}^{N} w_i \cdot \left(\frac{x_i - \bar{x}}{\sqrt{v}}\right)^3 \tag{3}$$

$$K = \sum_{i=1}^{N} w_i \cdot \left(\frac{x_i - \bar{x}}{\sqrt{v}}\right)^4 \tag{4}$$

where $w_i$ represents the weight, i.e., the fraction of biomass, of the $i$-th class with trait value $x_i$ in the sample at time $t$ and $N$ the number of classes. The normal distribution serves as benchmark and has per definition $S = 0$ and $K = 3$. Hence, large absolute values of $S$ and $K$-3 (excess kurtosis) imply that the shape of the distribution strongly deviates from a normal one. Small absolute values of $S$ indicate symmetric distributions whereas large negative or positive values of $S$ are related to distributions skewed to the left or right. For symmetric distributions, $K$ provides good information about the presence or absence of bimodality (DeCarlo 1997). Values of $K > 3$ characterize rather unimodal distributions with a pronounced peak around $\bar{x}$ and heavy tails (extreme values) while values of $K < 3$ result from less pronounced peaks, heavy shoulders ($\bar{x} \pm \sqrt{v}$) and lighter tails indicating bimodality.

The absolute values of $S$ and $K$ are usually positively correlated (Wyszomirski 1992) making $S$ and $K$ not entirely independent from each other (Blest 2003; Dorić et al. 2009; Jones et al. 2011). That is, high values of $S$ and low values of $K$ (bimodality) rule out one another, as a distribution with two distant maxima of similar magnitude cannot be highly skewed. Therefore, we jointly considered $S$ and $K$ to evaluate the shape of the trait distributions and allocated all trait distributions into one of the following four categories: (1) normal, (2) peaked, (3) skewed, or (4) bimodal, based on the threshold values outlined below. Distributions falling into the first three categories were conservatively considered as unimodal although skewed ones may express substantial side peaks or a pronounced shoulder.

First, we distinguished between normal and non-normal trait distributions based on a functional relationship between $S$ and $K$ entailed in the Jarque-Bera-Test-Statistic (Jarque and Bera 1987) frequently used to test for the normality assumption:

$$C_1 = S^2 + ((K-3)/2)^2. \tag{5}$$

The index $C_1$ equals zero for the normal distribution ($S = 0$, $K = 3$) and 9/25 for well-known non-normal distributions such as the uniform ($S = 0$, $K = 9/5$), the logistic ($S = 0$, $K = 21/5$) and the gamma distribution with $\alpha = 13$ ($S = 0.55$, $K = 3.46$,). Hence, we categorized a trait distribution as normal for $C_1 \leq 9/25$ and otherwise ($C_1 > 9/25$) as non-normal.

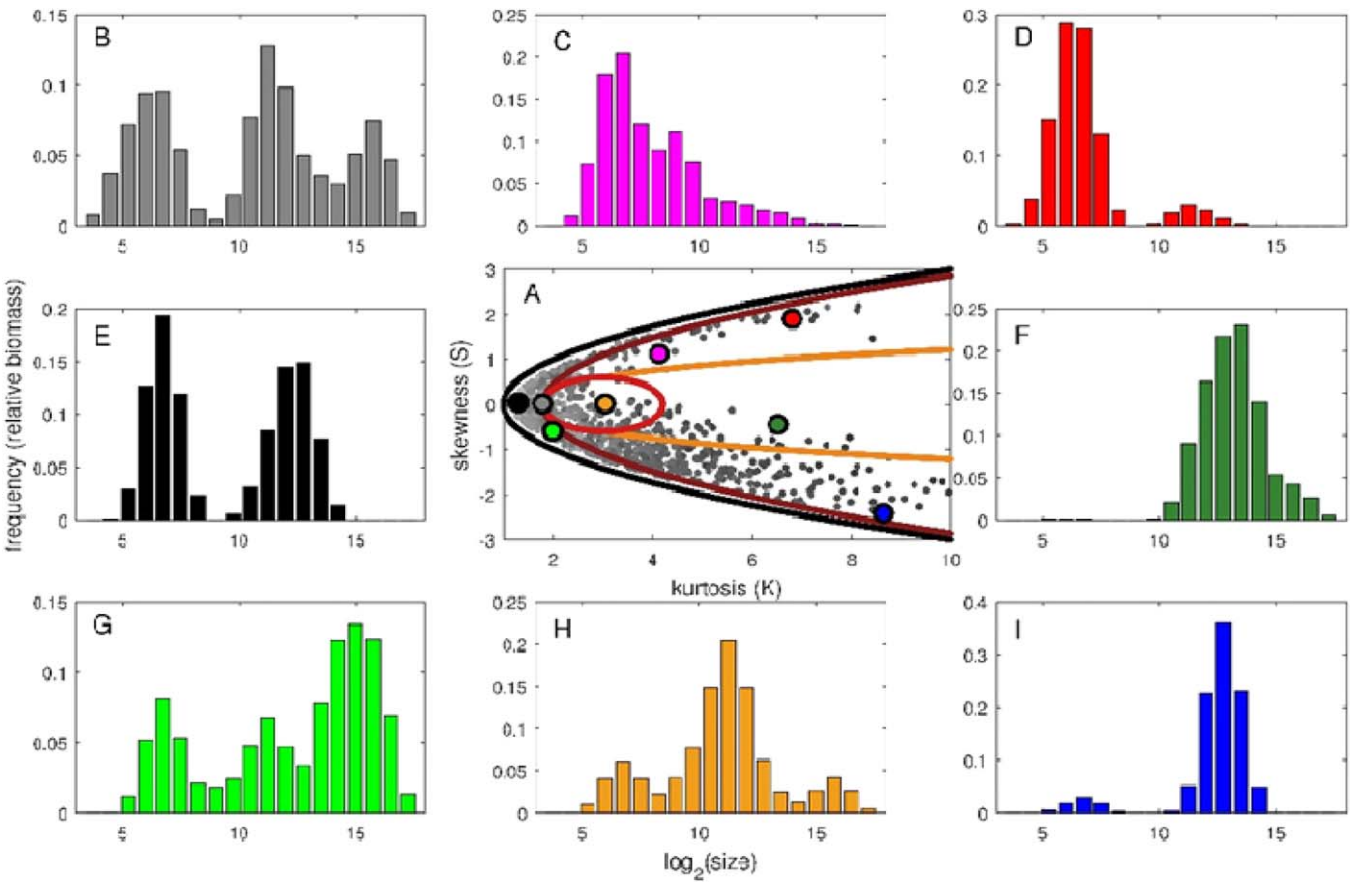


**Fig. 1.** (**A**) Characterization of the observed trait distributions of phytoplankton cell size in L. Constance according to their skewness, *S*, and kurtosis, *K*. $S \approx 0$ indicates rather symmetric distributions and $S > 0$ ($S < 0$) skewness to the right (left). $K < 3$ results from distributions with heavier shoulders than normal distributions and $K > 3$ from more peaked ones with small shoulders but heavy tails (extreme values). With increasing variance, the color of the dots changes from dark to light gray. The outer black line encompasses the mathematically feasible range of *S*–*K* values, the inner red circle the range for normal distributions following the index C1, *S*–*K* combinations more extreme than the outer brown line are classified as bimodal (index C2) and values falling within the inner orange line as peaked (index C3). *S*–*K* combinations falling between the C2 (brown) and C3 (orange) isoclines are considered as skewed (for details *see* "Materials and procedures"). The colored dots refer to the size distributions depicted in **B**–**I**. (**B**–**I**) Examples of observed distributions selected from different locations in the *S*–*K* plane which were classified as uniform (**B**, at the threshold to bimodal), skewed (**C**, **D**, **I**), bimodal (**E**, **G**), peaked (**F**), or normal (**H**). These examples represent the respective observed trait distributions which are closest to predefined combinations of *S* and *K* indicated by the colored dots in (**A**). Note the different scales of the *y* axes.

We further categorized the non-normal trait distributions according to their prevalent properties of peakedness, skewness, or bimodality by considering Pearson's *S*-*K* difference (Pearson 1929):

$$C_2 = S^2 - (K-3). \tag{6}$$

We considered a trait distribution as bimodal for $C_2 > 6/5 = 1.2$. This is the value of $C_2$ for the uniform distribution ($S = 0$, $K = 9/5$) which can be considered as a transition stage from symmetric unimodal to bimodal distributions. Indeed, $C_2$ has to be smaller than 1.2 in case of symmetric unimodal distributions and cannot be larger than $186/125 = 1.49$ for any asymmetric unimodal trait distribution (Klaassen et al. 2000). To be consistent with the threshold value for $C_1$, we chose the former value for $C_2$ but our overall results and conclusions also hold for more restricted conditions (Supporting Information Appendix A).

Finally, we used a modification of Sarle's bimodality coefficient (Pfister et al. 2013) to differentiate between skewed and peaked distributions:

$$C_3 = \left(S^2+1\right)^2 / K. \tag{7}$$

We categorized a trait distribution as skewed or peaked when $C_3$ is larger or smaller than $1156/1875 = 0.62$, respectively. The latter value results when aiming for consistency with the other threshold values. Overall, this resulted in the framework depicted in Fig. 1 where we classified our trait distributions based on combinations of *S* and *K* that jointly satisfy conditions derived from the well-known mathematical relationships between *S* and *K* provided above. The three

isoclines within the *K*-*S*-phase space represent combinations of *K* and *S* values that yield the same threshold values of $C_1$, $C_2$, and $C_3$ and are used to separate groups of trait distributions with shared properties. In contrast to numerous other approaches evaluating, e.g., the normality of a distribution, this approach does not require to specify the number of cells counted which was unknown for most of the sampling dates and may vary along the trait range. It is also well suited for distributions such as biomass-weighted frequency distributions in which each observation has a different weight. As our framework does not allow testing for significance as this would generally require information about the number of observations, we also tested for potential relationships between $\bar{x}$ and *S*, and between *v* and *K* for the different traits and water bodies. If the observed trait distributions would originate from normal distributions, their skewness and excess kurtosis (i.e., *K*-3) should fluctuate around zero independently of $\bar{x}$ and *v* (cf. Eqs. 1–4).

**Evaluating the quality of the aggregate model approach**

Temporal changes in the aggregated properties, i.e., total biomass, $B_T$, trait mean, $\bar{x}$, and standing trait variance, *v*, of a community consisting of *N* species (i.e., the full trait distribution) can be described by accounting for the dynamics of each species separately:

$$\frac{dB_i}{dt} := R(x_i) \cdot B_i \tag{8}$$

where $R(x_i)$ represents the per-capita net-growth rate and thus fitness function of the *i*-th species with biomass $B_i$ and trait value $x_i$ at sampling date *t*. This approach, is subsequently called *full model*, as it accounts for all details in our discrete trait distributions by using a correspondingly high number of species. We calculated separately for each sampling date the rates of change of the species biomasses based on the trait distribution observed at sampling date *t*. The temporal changes of the aggregate properties are described by (for derivation *see* Supporting Information Appendix B):

$$\frac{dB_T}{dt} := B_T \cdot \sum_{i=1}^{N} w_i \cdot R(x_i) \tag{9a}$$

$$\frac{d\bar{x}}{dt} := \sum_{i=1}^{N} w_i \cdot R(x_i) \cdot (x_i - \bar{x}) \tag{9b}$$

$$\frac{dv}{dt} := \sum_{i=1}^{N} w_i \cdot R(x_i) \cdot (x_i - \bar{x})^2 - v \cdot \sum_{i=1}^{N} w_i \cdot R(x_i) \tag{9c}$$

where $w_i$ denotes the relative biomass of the *i*-th species at time *t*.

Aggregate models approximate the temporal dynamics of $B_T$, $\bar{x}$, and *v* by making assumptions about the shape of the trait distribution and the linearity of the fitness function. We compare four aggregate models which differ in their approximations of the trait distribution and fitness function. We first consider two aggregate models, which describe the temporal dynamics of $B_T$ and $\bar{x}$ by a first-order approximation of Eq. 9 (Wirtz and Eckhardt 1996; Brandt et al. 2012; Wirtz 2013):

$$\frac{dB_T}{dt} \approx B_T \cdot R(x)|_{x=\bar{x}} \tag{10a}$$

$$\frac{d\bar{x}}{dt} \approx v(\bar{x}) \cdot \left.\frac{\partial R(x)}{\partial x}\right|_{x=\bar{x}} \tag{10b}$$

Equation 10b includes the second central moment, i.e., the trait variance *v*, which temporal dynamics are not described by an equation. Hence, we have to close this system of differential equations by assuming *v* either to be constant (Wirtz and Eckhardt 1996; Merico et al. 2014) or to be well expressed in terms of the lower central moment, $\bar{x}$ (Wirtz and Lemmen 2003). In general, such moment closure methods are based on assumptions about the shape of the trait distributions. In the first case, we set *v* equal to the average of the observed trait variances. This approximation, labeled *constant variance*, is exact for linear fitness functions combined with symmetric trait distributions (i.e., $S = 0$) (Abrams et al. 1993).

In the second case, we assumed a unimodal relationship between *v* and $\bar{x}$ and thus perform a *data-based moment closure* by fitting a parabolic function to our data:

$$v(\bar{x}) = a_1(\bar{x} - a_2)(\bar{x} - a_3) \tag{11}$$

This approximation is exact for linear fitness functions and communities that comprise only two distinct phenotypes with the trait values $x_{min}$ and $x_{max}$ (Wirtz and Eckhardt 1996; Cortez 2011; Ellner and Becks 2011) in which case the parameters $a_1$, $a_2$, and $a_3$ equal 1, $x_{min}$ and $x_{max}$, respectively.

As a second approach, we consider two aggregate models which describe the temporal dynamics of $B_T$, $\bar{x}$ and *v* combined with a second-order approximation of Eq. 9 (Wirtz and Eckhardt 1996; Norberg et al. 2001; Merico et al. 2009; Coutinho et al. 2016). These models consider additionally the dynamics of *v* and enable a better approximation of the non-linearity of the fitness function by including its second derivative and of the shape of the trait distribution by accounting for potential skewness and kurtosis:

$$\frac{dB_T}{dt} \approx B_T \cdot \left( R(x)|_{x=\bar{x}} + v \frac{1}{2} \left.\frac{\partial^2 R(x)}{\partial x^2}\right|_{x=\bar{x}} \right) \tag{12a}$$

$$\frac{d\bar{x}}{dt} \approx v \left.\frac{\partial R(x)}{\partial x}\right|_{x=\bar{x}} + M_3 \frac{1}{2} \left.\frac{\partial^2 R(x)}{\partial x^2}\right|_{x=\bar{x}} \tag{12b}$$

$$\frac{dv}{dt} \approx M_3 \left.\frac{\partial R(x)}{\partial x}\right|_{x=\bar{x}} + (M_4 - v^2) \frac{1}{2} \left.\frac{\partial^2 R(x)}{\partial x^2}\right|_{x=\bar{x}} \tag{12c}$$

In general, this approximation is valid when *v* is small or when the non-linearity of the fitness function is only weak (cf. Supporting Information Appendix B). Equations 12b and

12c include the third ($M_3$) and fourth ($M_4$) higher central moments which have to be expressed in terms of lower moments to close this system of differential equations. We compare the results of two different moment closure techniques. First, we assume the trait distribution to be normal (Wirtz and Eckhardt 1996; Merico et al 2009). In this case $M_3 = 0$ and $M_4 = 3 \cdot v^2$. Second, similar to Norberg et al. (2001) we perform a data-based moment closure based on linear regressions between the absolute ($S$ vs. mean) or log-transformed ($K$ vs. $v$) values of the standardized central moments:

$$\begin{aligned} S &= a \cdot \bar{x} + b \\ \ln(K) &= d \cdot \ln(v) + \ln(c) \end{aligned} \quad (13)$$

Hence, in accordance with Norberg et al. (2001), power-functions of the lower moments express the higher moments:

$$\begin{aligned} M_3 &= S \cdot v^{3/2} = a \cdot \bar{x} \cdot v^{3/2} + b \cdot v^{3/2} \\ M_4 &= K \cdot v^2 = c \cdot v^{d+2} \end{aligned} \quad (14)$$

To evaluate the quality of these four aggregate models we calculated the rates of change of the aggregate properties according to Eqs. 9, 10, and 12 for the observed distributions of size and maximum length by assuming two types of fitness functions $R(x)$ differing in their non-linearity. Afterwards we compared these results to the ones of the full trait distribution model.

The first fitness function we used is a standard allometric relationship between the species maximum growth rate, and logarithmic cell size $x$, i.e., $R(x) = m \cdot (2^x)^{-0.25}$. To establish realistic values for the range of maximum growth rates within phytoplankton communities we chose the scaling parameter $m$ to take a value of 3. The second fitness function relies on the maximum length of the algal cells, which is linked more closely to the top-down control of the phytoplankton. Consumers can only exploit a limited prey spectrum, which can be linked to the maximum cell length. We assumed grazing by a diverse zooplankton community that prefers small phytoplankton over large ones and hence conservatively a rather gradual decline with maximum length. Hence, as a second fitness function, we chose a logistic function according to $R(x) = 1\text{-}(1 + \exp(\alpha(x\text{-}\beta)))^{-1}$. The parameter $\alpha$ describes how fast the transition from edible to less edible species occurs and was set to 1. The parameter $\beta$ reflects the upper threshold of particle sizes, which can be processed efficiently by common herbivores such as daphnids in our habitats. We chose a value of $\log_2(45)$ $\mu$m for maximum length and $\log_2(1024)$ $\mu m^3$ for size (cf. Burns 1968; Lampert 1978).

We expressed the model performance as the ratio between the rates of change of the aggregate properties of the aggregate (Eqs. 10 or 12) and full (Eq. 9) models for the individual trait distributions. For example, to evaluate the performance of the aggregate models with a second order approximation we computed the ratios $(dB/dt)_{aggregate}/(dB/dt)_{full}$ (Eqs. 12a and 9a), $(d\bar{x}/dt)_{aggregate}/(d\bar{x}/dt)_{full}$ (Eqs. 12b and 9b) and $(dv/dt)_{aggregate}/(dv/dt)_{full}$ (Eqs. 12c and 9c). For positive ratios, the median of $2^{|\log2(ratios)|}$ was used as an average factor across all trait distributions giving equal weight to over- and underestimations. In addition, we provide the share of negative ratios implying that the aggregate model predicts temporal changes into the wrong direction, which only occurred for the variance dynamics.

## Assessment

### Classifying the shape of observed trait distributions

Our classification scheme involves a comprehensive characterization of the shape of the trait distributions by considering $S$ and $K$ in concert (Fig. 1A, for details *see* "Characterizing trait distributions based on their shape" section). The shape of the distributions differed between both traits and habitats, varied greatly in time and covered the full range from strongly multimodal to peaked and rather symmetric to pronouncedly skewed in either direction (Fig. 1, Supporting Information Appendix C, Figs. C1–C3; Table 1) as similarly found by Downing et al. (2014). The size distributions in LC were mostly characterized as skewed (44%) or bimodal (36%) and rarely as normal (13%) or peaked (7%). In SR peaked size distributions (40%) prevailed together with skewed (31%) and normal ones (25%). This is in line with the mostly highly diverse phytoplankton community of LC (Weithoff et al. 2015) yielding on average higher trait variances than in SR (Table 1). Phytoplankton biomasses were distributed usually across a major part of the entire trait range. This holds in particular for maximum length in both habitats and for size in Lake Constance (LC) whereas size distributions in Saidenbach Reservoir (SR) were typically restricted to a more narrow range (Table 1; Fig. 1, Supporting Information Appendix D, Fig. D1) due to the frequently dominating pennate diatoms (Horn et al. 2011). In fact, length distributions in LC showed the largest diversity in the shape from all traits and habitats (37% normal, often relatively small absolute values of $S$, and $K$ values relatively close to 3) whereas in SR 92% of the length distributions were (extremely) skewed or bimodal and exhibited large variances. The large difference in the shape between the two trait distributions in SR originates from the elongated shape of the diatoms. Their cell size (i.e., volume) is similar to that of many co-occurring, more spherical species resulting in peaked size distributions. In contrast, their maximum length is much larger than that of most other species yielding heavily skewed or bimodal length distributions.

### Testing the reliability of the moment-based classification method

Our classification scheme depends on defining threshold values based on relationships between $S$ and $K$ (cf.

**Table 1.** Temporally averaged mean trait values, $\bar{x}$, mean standing variance, $v$, standardized by the respective maximum variance (45 for size and 18 for maximum length), mean absolute values of the skewness, $S$, and the kurtosis, $K$ (all values with ± one STD reflecting the temporal variation), frequencies in % of the different types of distributions, and Pearson's linear correlation coefficients for $\bar{x}$ vs. $S$, ln($v$) vs. ln($K$), and $\bar{x}$ vs. $v$ for the traits size in $\log_2$ ($\mu m^3$) and maximum length in $\log_2$ ($\mu m$) in L. Constance (LC, 1979–1999, $n = 853$) and Saidenbach Reservoir (SR, 1975–2011, $n = 1259$).

| *Trait/habitat* | $\bar{x}$ | $v/v_{max}$ | $\lvert S \rvert$ | $\lvert K\text{-}3 \rvert$ |
|---|---|---|---|---|
| LC size | 10.8 ± 1.7 | 0.14 ± 0.06 | 0.85 ± 0.6 | 1.7 ± 2.0 |
| SR size | 9.9± 1.1 | 0.06 ± 0.05 | 0.6 ± 0.5 | 2.0 ± 2.0 |
| LC length | 5.1 ± 1.0 | 0.11 ± 0.07 | 0.6 ± 0.5 | 1.4 ± 1.9 |
| SR length | 6.4 ± 0.9 | 0.13 ± 0.08 | 1.8 ± 1.4 | 6.5 ± 10.8 |
| ***Trait/habitat*** | ***Normal*** | ***Peaked*** | ***Skewed*** | ***Bimodal*** |
| LC size | 13 | 7 | 44 | 36 |
| SR size | 25 | 40 | 31 | 4 |
| LC length | 37 | 12 | 35 | 16 |
| SR length | 4 | 4 | 51 | 41 |
| ***Trait/habitat*** | $r^2$ *of* $\bar{x}$ *vs. S* | $r^2$ *of ln(v) vs. ln(K)* | | $r^2$ *of* $\bar{x}$ *vs. v* |
| LC size | 0.73 | 0.72 | | 0.26 |
| SR size | 0.09 | 0.37 | | 0.11 |
| LC length | 0.34 | 0.44 | | 0.15 |
| SR length | 0.69 | 0.72 | | 0.25 |

"Characterizing trait distributions based on their shape" section) but their exact values had little influence on our overall results (Supporting Information Appendix A). The classification of the different types of non-normal distributions was in line with the magnitudes of the variance, $v$, $S$, and $K$, and the relationships among lower and higher moments (Fig. 2; Table 1). For example, the highest fraction of distributions classified as peaked (40% for size in SR) coincides with the smallest standardized variance, and the highest fractions of skewed (51%) and bimodal distributions (41%, length in SR) are associated with high $v$, maximum absolute values in $S$ and $K$ and strong correlations among lower and higher moments. The sign of $S$ changed highly significantly ($p < 0.001$) from positive to negative with increasing values of $\bar{x}$, for both traits in both habitats (Fig. 2A–D; Table 1). $K$ was also clearly related to $v$ ($p < 0.001$) (Fig. 2E–H; Table 1). These relationships were particularly strong ($r^2$: 0.69–0.73) if a low percentage of trait distributions was classified as normal (13% for size in LC and 4% for length in SR). In contrast, when we obtained a relatively high share of normal distributions (37% for length in LC) combined with a rather even occurrence of the other types of shape, the different moments had intermediate values with relatively high standard deviations and exhibited only moderately strong correlations among each other (Table 1). These differences in correlation strength among lower and higher moments support the reliability of our classification scheme as for trait distributions originating from normal distributions $S$ and excess kurtosis ($K$-3) should fluctuate by definition around zero independently of $\bar{x}$ and $v$. This implies that a high percentage of normal distributions should coincide with weaker correlations among lower and higher moments that is in line with our data.

### Tight relationships between lower and higher moments allow a data-based moment closure

The relationships between the four moments can be used to improve the accuracy of aggregate models using a data-based moment closure. First-order approximations require expressing $v$ as a parabolic function of $\bar{x}$ (for details *see* "Evaluating the quality of the aggregate model approach" section). Such a unimodal relationship is to be expected given the usually restricted trait ranges in natural communities because extreme values of $\bar{x}$ can only arise if most of the biomass clusters at very small or high trait values, implying a small variance. In contrast, intermediate mean trait values can be associated with narrow or broad trait distributions and, thus, small or large variances, respectively. Our data reveal in principal a unimodal envelope for the relationship between the maximum variance and $\bar{x}$ (Supporting Information Appendix D, Fig. D1). However, the scatter around fitted parabolic relationships was high ($r^2 = 0.11$–$0.26$) and in two cases only the ascending part of the parabolic function was relevant (size in SR and length in LC). The temporal variability in $v$ (Fig. 2E–H) also reveals the limited potential to approximate the observed variances by their constant mean value, as done in one of the first-order approaches. Furthermore, second-order approximations require expressing $K$ and $S$ as functions of $\bar{x}$ or $v$ (for details *see* "Evaluating the quality of the aggregate model approach"). In line with the low share of normal distributions and the tight relationships between $\bar{x}$ and $v$, we found strong correlations between S and $\bar{x}$, and K and $v$, for size in LC and maximum length in SR (Table 1). These relationships arise from the fact that within a limited trait range as it exists in our and presumably most communities, small values of $\bar{x}$ can only occur if organisms with small trait values clearly dominate the biomass. This results in a trait distribution skewed to the right ($S > 0$) as long as some organisms with larger trait values are still present (e.g., Fig. 1C) and vice versa (e.g., Fig. 1I). In addition, the negative correlation between $v$ and $K$ results from the fact that peaked trait distributions with high $K$ and thus pronounced tails can only arise for smaller $v$ within a limited trait range (e.g., Fig. 1F). In line, $v$ can only be large for uniform (e.g., Fig. 1B) or multi- or bimodal distributions (e.g., Fig. 1E). Such distributions imply low values of $K$ due to flat peaks with heavy shoulders or distinct peaks at both extremes.

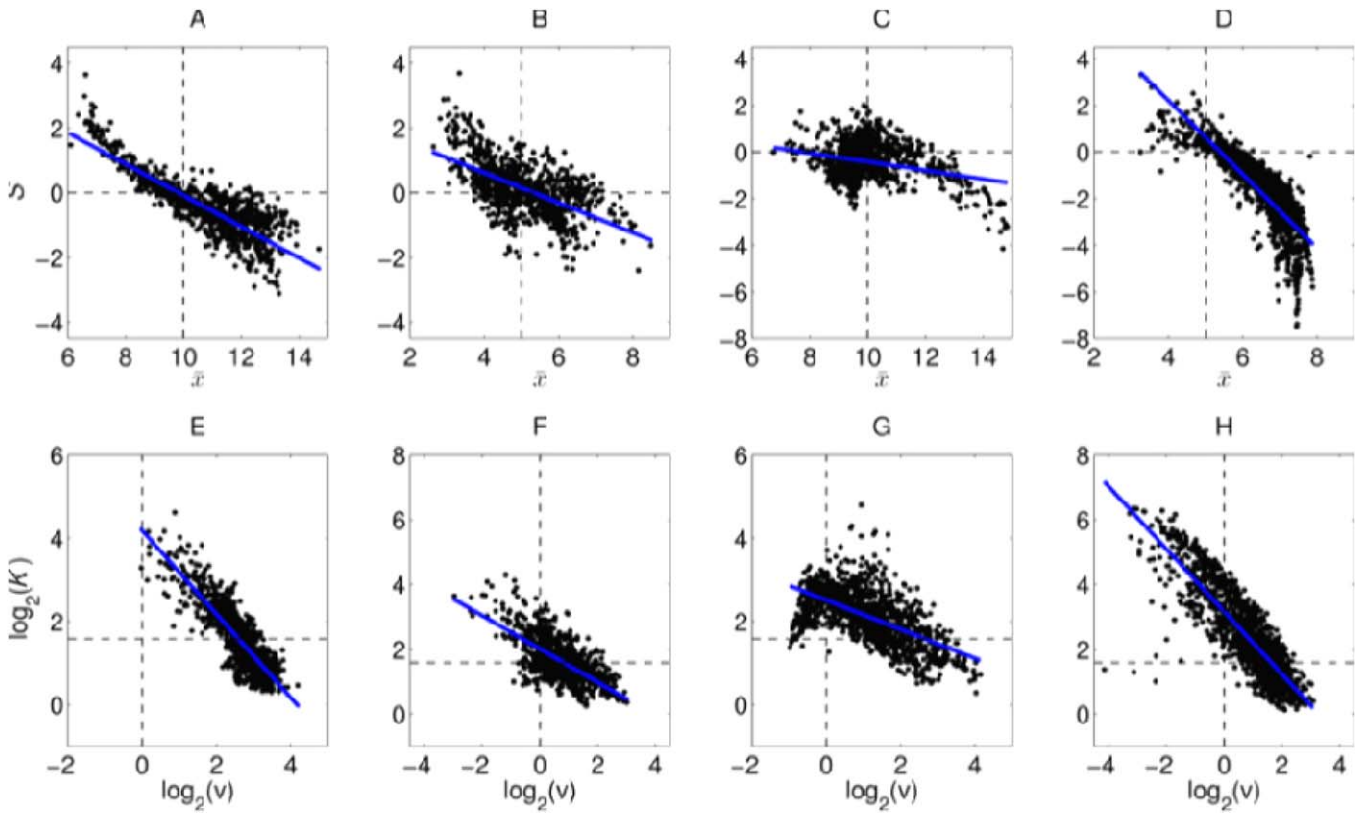


**Fig. 2.** Correlations between the skewness, *S*, and (**A**) size ($r^2 = 0.73$) and (**B**) maximum length ($r^2 = 0.34$) in L. Constance and (**C**) size ($r^2 = 0.09$) and (**D**) maximum length ($r^2 = 0.69$) in Saidenbach Reservoir, and between $\log_2$ of the kurtosis, *K*, and variance, *v*, of (**E**) size ($r^2 = 0.72$) and (**F**) maximum length ($r^2 = 0.44$) in L. Constance and (**G**) size ($r^2 = 0.37$) and (**H**) maximum length ($r^2 = 0.72$) in Saidenbach Reservoir of the observed trait distributions of phytoplankton. Note the differences in the scales of the axes.

To conclude, as exemplified by the size distributions in LC and the length distributions in SR the remarkable fact arises that strong correlations among moments on one side point to major deviations from normality but on the other hand imply a large potential to correct for the impact of *v*, *S*, and *K* using a data-based moment closure. Subsequently, we test whether this holds when confronting the aggregate models with real data.

**Comparing the performance of aggregate models with normal- or data-based moment closures**

We tested the performance of the different aggregate models by evaluating the deviations of their predictions from the results of a corresponding full model using the observed trait distributions. We combined the observed size distributions with an allometric relationship of the growth rate representing a weakly non-linear fitness function, and the length distributions reflecting grazing resistance with a logistic function yielding a moderate non-linearity with a turning point. This reflects that cell size determines the growth rates of phytoplankton and maximum length their edibility and thus loss rates. As this provokes a confounding between the type of trait distribution and the type of non-linearity we abstracted from the ecological context and calculated also the aggregate model performance combining the size distributions with the logistic function and the length distributions with the allometric relationship (Supporting Information Appendix E). For the sake of clarity, the latter data are not described in detail, as they did not change the overall patterns described below.

Independent of the type of non-linearity, the aggregate models consistently approximated the changes of the community biomasses, $dB_T/dt$, better than the changes of the mean trait values, $d\bar{x}/dt$, which, in turn, were more accurately predicted than the changes of the standing variances, $dv/dt$ (Fig. 3). In addition, the second-order approximations delivered consistently more accurate (or similar, Fig. 3J) results than the first-order approximations for the biomass and trait changes (Fig. 3). For example, for size and the weak non-linearity, $dB_T/dt$ of the aggregate models deviated from the full models on average (for details *see* "Evaluating the quality of the aggregate model approach" section) by a factor of 1.1 (LC) and 1.03 (SR) when using first-order approximations. The corresponding values are only 1.01 (LC) and 1.001 (SR) when employing second-order approximations. For large *v*, as found for size in LC and maximum length in both

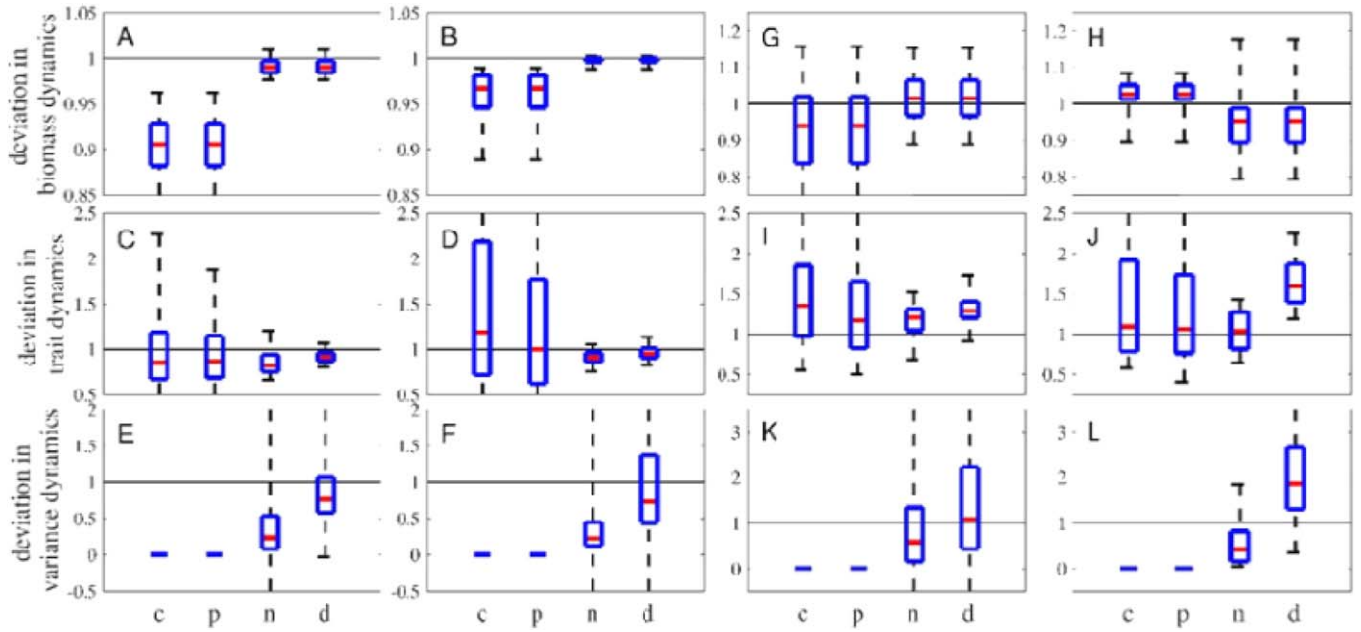


**Fig. 3.** Deviation of the four different types of aggregate models from the respective full models expressed as the ratio between aggregate and full model in respect to the rates of biomass ($[dB/dt]_{aggregate}/[dB/dt]_{full}$; (**A**, **B**, **G**, **H**), trait ($[d\bar{x}/dt]_{aggregate}/[d\bar{x}/dt]_{full}$; **C**, **D**, **I**, **J**) and variance ($[dv/dt]_{aggregate}/[dv/dt]_{full}$; **E**, **F**, **K**, **L**) changes at the individual sampling dates. They are based on a weakly non-linear allometric relationship (fitness function) and the size distributions from Lake Constance, LC (**A**, **C**, **E**) and Saidenbach Reservoir, SR (**B**, **D**, **F**), and a moderately non-linear, logistic relationship and the distributions of maximum length from LC (**G**, **I**, **K**) and SR (**H**, **J**, **L**). Labeling of the *x* axis: c stands for the aggregate model with constant variance, p for the one with a parabolic relationship between trait mean and variance (both first-order approximations), and n and d for the second-order approximations based on normality or data. The blue boxes represent the 25% and 75% quartiles with the median (red horizontal bar) and the whiskers reflecting the 5% and 95% quartiles of all sampling dates which are partially truncated to improve the clarity of the figure. A ratio of 1 implies a perfect fit between the approximated values derived from aggregate models and the full model. Values $< 0$ arise if the aggregate model predicts changes in the wrong direction. By definition, the variance is constant (i.e., its rate of change is 0) for the first-order moment closures and the types of moment closures do not affect $dB/dt$, i.e., the values are identical within the first- and second order approximations. Note the different scales of the *y*-axes.

habitats, $\bar{x}$ provides a less suitable representation of the entire trait distribution. This results in larger deviations for $dB_T/dt$ that could be strongly reduced by the second-order approximations (Fig. 3).

We found similar patterns but stronger deviations for $d\bar{x}/dt$. The models deviated on average by a factor of 1.4 (constant variance) and 1.3 (data-based variance, LC) and 1.8 and 1.7 (SR) for the first-order approximations and only by 1.2 (normal-based) and 1.1 (data-based) (LC) and 1.1 and 1.1 (SR) for the second-order approximations using the weak non-linearity. The differences can be attributed to the large temporal variability of $v$ and S (Figs. 2, 3B) for which first-order approximations do not account for. Accordingly, both second-order approximations greatly improved the fit. This holds in particular for the data-based moment closure (Fig. 3, Supporting Information Appendix E) which accounted for $S$ and $K$. Based on the tight relationships between $S$ and $\bar{x}$, and $K$ and $v$ the data-based moment closure strongly reduced the deviations compared to the predictions of the normal-based aggregate model. Remarkably, the second-order approximation with a normal-based moment closure was better than the first-order approximations for most data points even when many trait distributions were (strongly) non-normal (Fig. 3A–D, G–J). This happens because both second-order approximations account at least partially for the non-linearity of the fitness function and the actual values of $v$.

Under certain conditions, second-order approximations may also predict the variance dynamics, $dv/dt$, reasonably well but in our case, the predictions of $dv/dt$ from the aggregate models strongly deviated from the results of the full models already for the weak non-linearity (Fig. 3E,F). Even the direction of the changes in $v$ (i.e., the sign of $dv/dt$) was falsely predicted for 21% (LC) and 12% (SR) of the size distributions and for 45% (LC) and 12% (SR) of the length distributions by the normal-based approximation (Fig. 3K,L). For the data-based approach, the corresponding values are 5% (LC) and 12% (SR) for size and 29% (LC) and 5% (SR) for length. For data points with a correct sign, $dv/dt$ deviated on average by a factor of 3.5 (LC) and 4.1 (SR) for the size distributions and of 2.8 (LC) and 9 (SR) for the length distributions for the normal-based moment closure. The data-based moment closure reduced these factors substantially to 1.5 (LC) and 1.8 (SR) for the size distributions and to 2.2 (LC)

and 1.4 (SR) for the length distributions (cf. Supporting Information Appendix E, Fig. E1L). As expected, the greatest improvements were achieved when the correlations between lower and higher moments were most pronounced. Furthermore, the normal-based approach mostly underestimated $dv/dt$ when the sign was correct whereas the data-based approach was less biased (*see* also Supporting Information Appendix E). The latter implies that under- and overestimations at individual sampling dates may counteract each other in the long term whereas errors accumulate in the normal-based approach leading to an unrealistic decline of $v$.

As expected, the aggregate models usually performed better for the weak than for the moderate non-linearity (Fig. 3, Supporting Information Appendix E). For example, for size and the moderate non-linearity the deviations of $dB_T/dt$ increased to a factor of 1.13 (LC) and 1.14 (SR) when using a first-order approximation, and to a factor of 1.27 (LC) and 1.08 (SR) when employing a second-order approximation. For $d\bar{x}/dt$ the corresponding values are 1.5 and 1.6 (LC) and 2.1 and 1.8 (SR) for the first-order approximations, and 1.5 and 1.8 (LC) and 1.4 and 1.2 (SR) for the second-order approximations. The pattern was less consistent for $dv/dt$ deviating on average by a factor of 1.9 (LC) and 2.3 (SR) for the normal-based moment closure and by 2.4 (LC) and 2.7 (SR) for the data-based moment closure if the sign of $dv/dt$ was correct. Both approaches failed to predict the sign correctly for 12–15% (LC) or even 37% (SR) of the size distributions (Supporting Information Appendix E).

Comparing the two aggregate models based on the first-order approximation reveals only a slight improvement with a data-based moment closure which predicts the value of $v$ with a parabolic relationship from the actually observed value of $\bar{x}$ rather than using constantly the mean observed variance (Fig. 3C,D,I,J). This is in line with the large scatter around the parabolic relationship between $v$ and $\bar{x}$ (Supporting Information Appendix D, Fig. D1). Relating the two second-order approximations to each other delivers consistently a better fit by the data-based approach than by the one based on normality for the weak but not for the moderate non-linearity (Fig. 3). The data-based approach accounts for the impact of $S$ and $K$ on the estimates of $d\bar{x}/dt$ and $dv/dt$ which improved the latter in particular (*see* also Supporting Information Appendix E). However, in case of the moderate non-linear fitness function, higher derivatives strongly influenced the dynamics of the aggregate properties that were not accounted for by any of the aggregate models evaluated.

**Mechanisms underlying the deviations of the aggregate from the full models**

Considering the deviations of the aggregate from the full models in more detail reveals systematic patterns reflecting the underlying mathematical relationships. Without loss of generality, we exemplify them for the size distributions in LC and the weak non-linearity. The magnitude of the second and higher derivatives of the allometric relationship representing here the weak non-linearity strongly depends on the mean and thus the location of the trait distribution. However, the derivatives are all monotonically increasing or decreasing functions of the trait and thus their signs remain constant along the trait range. Hence, the rather simple curvature of the allometric relationship leads to a clear dependence of the deviations between aggregate and full model on the shape of the trait distributions described by their higher moments. For $dB_T/dt$ the first-order approximations which either kept $v$ constant or had little power to estimate changes in $v$ from $\bar{x}$, delivered deviations which strictly increased with $v$ (Fig. 4A,B; Supporting Information Appendix B, Eq. B5; Spearman rank correlation coefficient $\rho = -0.96$). Accordingly, the second-order approximations considering $v$ provided an almost perfect fit and the small deviations were tightly linked to the third moment (Fig. 4C,D; $\rho = 0.99$; cf. Supporting Information Appendix B, Eq. B5). Thus, $dB_T/dt$ was consistently underestimated due to the curvature of the allometric relationship (Jensen's inequality).

Deviations between aggregate models with first-order approximations and the full models in respect to $d\bar{x}/dt$ were again related to $v$, in particular for the approach assuming a constant $v$ (Fig. 4E; $\rho = -0.92$). The correlation between deviations and $v$ remaining in the data-based approach (Fig. 4F; $\rho = -0.70$) reveals that it accounted only partly for the effect of $v$ due to the lack of a distinct relationship between $\bar{x}$ and $v$ (Fig. D1). Deviations found in the second-order approximations were linked to the third moment both in the normal (Fig. 4G; $\rho = 0.90$) and to a lesser extent in the data-based approach (Fig. 4H; $\rho = 0.45$). In the normal-based approach, the third moment accounted for deviations from normality whereas in the data-based approach, the smaller deviations and weaker correlation with the third moment arise from the rather close fit between $\bar{x}$ and $S$ (Fig. 2A). Much of the remaining variation is attributable to $K$ and higher moments (cf. Supporting Information Appendix B, Eq. B10).

Considering $dv/dt$, the absolute values of the pronounced deviations between aggregate and full models declined with $K$, in particular when using the normal-based approach (Fig. 4I; $\rho = -0.91$). This reveals that $dv/dt$ is estimated reliably only for size distributions with $K \approx 3$. For rather broad ($K<<3$) or peaked distributions ($K>>3$) the normal-based moment closure strongly over- or underestimated $dv/dt$. The data-based approach strongly reduced the deviations (Fig. 3E,F) due to the tight relationship between $v$ and $K$ (Fig. 2E).

In contrast to the allometric relationship, both the sign and magnitude of the higher derivatives of the logistic function strongly depend on the relative location of $\bar{x}$ compared to the turning point of the logistic function. Hence, for the moderate non-linearity we did not find reliable correlations between the deviations and the higher moments but the deviations were non-linearly related to $\bar{x}$. Given the resulting

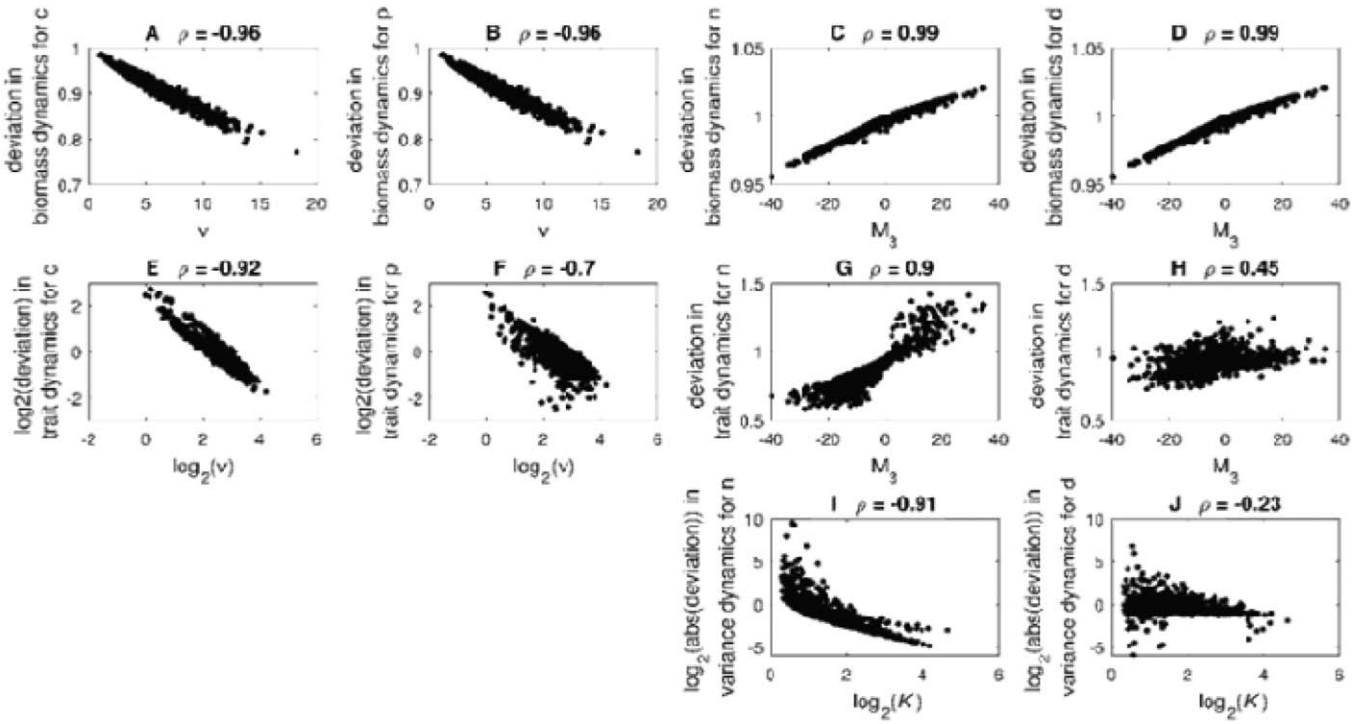


**Fig. 4.** Relationships between the deviation in the rates of the aggregate properties of the four different types of aggregate models from the respective full models and higher moments at the individual sampling dates for the observed size distributions in Lake Constance and the weak nonlinearity. The deviation is expressed as the ratio of the rates of biomass ($[dB/dt]_{aggregate}/[dB/dt]_{full}$; **A**–**D**), trait ($[d\bar{x}/dt]_{aggregate}/[d\bar{x}/dt]_{full}$; **E**–**H**) or variance ($[dv/dt]_{aggregate}/[dv/dt]_{full}$; **I**, **J**) changes of the aggregate model and the full model, respectively. The two aggregate models with first-order approximation are labeled c (constant variance; **A**, **E**) and p (data-based variance; **B**, **F**), and those with second-order approximation are labeled n (normal-based; **C**, **G**, **I**) or d (data-based; **D**, **H**, **J**). $\rho$ provides the respective values of the Spearman correlation coefficient. Note the different scales of the *y*-axes.

lack of generality details of those relationships are not shown.

## *Discussion*

We developed a novel approach to classify the critical shape properties of biomass-weighted trait distributions into four common types: normal, skewed, peaked, and bimodal. Our approach is easy to employ as it involves only the calculation of the first four moments and is robust with respect to the exact threshold values chosen (Supporting Information Appendix A). Furthermore, it does not demand to specify the number of items counted which is typically unknown or uneven across the trait range in plankton counts, and will be rather insensitive to the exact number of classes chosen along the trait axis. This method goes beyond purely testing for a distinct type of distribution such as normality. It enables spatial-temporal and cross-system comparisons with respect to the predominant shapes of trait distributions and investigations of changes in the predominant selection pressure.

In accordance with highly skewed and multimodal size and length distributions of aquatic invertebrates (Zimmer et al. 2001), birds, and insects (Griffiths 1986) our method classified a low share of observed phytoplankton trait distributions as normal. This is in line with the pronounced correlations between mean, $\bar{x}$, and skewness, $S$, and variance, $v$, and kurtosis, $K$, which is likely generalizable across systems where traits are restricted to a finite range. These relationships represent two sides of one coin: on the one side, normal trait distributions cannot be assumed as the rule when the trait distributions observed at a given date or location cover a substantial part of the entire possible trait range. This feature is to be expected unless substantial parts of the community under consideration are entirely absent in numerous samples. Thus, our data question the realism of the simplifying assumption made by numerous aggregate models that trait adjustments proceed through a shift in the mean trait value while the variance or shape of the trait distribution remain unchanged (Supporting Information Appendix F, Fig. F1). A more realistic abstraction for restricted trait ranges is that not only the mean and partly the variance but also the shape varies in time, leading to correlations among the lower and higher moments (Supporting Information Appendix F, Fig. F1). On the other side, strong correlations between $S$ and $\bar{x}$, and $K$ and $v$ may strongly improve the performance of aggregate models using a second-order approximation and a data-based moment

closure. We demonstrate these two counteracting processes by comparing the aggregate approaches for different trait distributions and aggregate properties. For example, the size distributions of LC were characterized by a high $v$ and pronounced deviations from normality but at the same time had strong correlations among the lower and higher moments (Table 1). Accordingly, the data-based moment closure was in reasonable agreement with the full model for biomass and trait dynamics despite the high variance and delivered more reliable approximations than approaches with first-order approximations or a normal-based moment closure (Fig. 2).

Based on 4200 trait distributions we tested the performance of four aggregate model approaches for a weakly and a moderately nonlinear fitness function, which are used frequently to describe growth and loss processes (Peters 1983; Lampert and Sommer 2007). The deviations between the aggregate and full models depended on all five factors investigated: the aggregate property considered (i.e., the changes in the biomass, trait, or variance), the strength and curvature of the non-linearity in the fitness function, the type of aggregate model, the variance, and the shape of the trait distribution. We found distinct patterns for the first two factors: The quality of the fit consistently declined from the biomass to the trait dynamics and particularly to the variance dynamics, and with increasing non-linearity of the fitness function as expected from theory (Savage et al. 2007; Merico et al. 2009). The impact of the other three factors was more complex and context dependent. The patterns in the deviations clearly reflected the mathematics underlying the respective model approaches in concert with the properties of the trait distributions (Fig. 4). Overall, most deviations correlated strongly with the next higher moment or derivative not considered in the respective approach.

Considering the weak non-linearity, $dB_T/dt$ estimated with first- or second-order approximations deviated on average by 0.1–10% from the full model. This may appear acceptable given the usual uncertainties in parameter estimates. It should, however, be acknowledged that we judged the performance of the aggregate models separately for distinct points in time and separately for $dB_T/dt$, $d\bar{x}dt$ and $dv/dt$ for the sake of generality and clarity. This neglects a potential accumulation of errors in time that may lead to substantial differences in the long run and disregards the consequences of potential deviations in one aggregate property for the others through potential feedbacks. For example, $v$ influences the speed of trait adaptation, $d\bar{x}dt$, which describes the adjustment to altered environmental conditions such as predator and prey biomasses (Tirok et al. 2011). Hence, studies on biomass-trait dynamics are sensitive to a correct estimation of $v$ and the changes thereof, $dv/dt$, as their results often depend on the relative speed of biomass (indicating ecological dynamics) and trait changes (may indicate evolutionary dynamics), i.e., on the magnitude of $dB_T/dt$ and $d\bar{x}dt$ (cf. Saloniemi 1993; Dercole et al. 2006; Mougi 2012). Predicting $v$ and $dv/dt$ reliably is also highly relevant in the context of functional biodiversity research and of the maintenance of biodiversity in particular.

Unfortunately, predictions of all aggregate approaches were prone to often substantial errors with respect to $dv/dt$ even for a weakly non-linear fitness function. Furthermore, the normal-based approach mostly underestimated $dv/dt$ when the sign was correct (Fig. 3). Given the positive sign of the second derivative of the allometric function, this implies an underestimation of the increase of $v$. This is in line with the overall tendency of $v$ to decline in aggregate models previously explored in other studies (Merico et al. 2009; Coutinho et al. 2016). To counteract this permanent loss of functional diversity and thus adaptive potential, previous studies had to maintain $v$ by other processes such as immigration or diffusion terms or more complex trade-offs, all demanding additional assumptions (Wirtz and Eckhardt 1996; Norberg et al. 2001; Merico et al. 2014; Tirok et al. 2011). It shows that even for weakly non-linear fitness functions the normal-based model approach may not be able to reflect changes in biodiversity realistically. This is supported by a recent model study where a normal-based aggregate model overestimated the time scale of the biomass and trait dynamics by a factor of 10 when assuming rather smooth fitness functions (Coutinho et al. 2016).

For the moderately non-linear logistic fitness function, the aggregate models often failed (Fig. 3, Supporting Information Appendix E) since even second-order approximations with a data-based moment closure could not capture such a curvature. The higher derivatives of the fitness function for which none of the aggregate models accounts, limited the model accuracy more strongly than the type of moment closure, i.e., the actual representation of the shape of the trait distribution. This was particularly true for $dv/dt$ for both, the normal- and the data-based approach but deviations for $dB_T/dt$ and $d\bar{x}dt$ were generally also much larger than for the weak non-linearity.

A potential solution to improve the performance of trait-based models while maintaining their operability in particular for moderately or strongly nonlinear fitness functions or trait distributions with high variance are "hybrid" models. They attempt neither, to describe the entire population or community only by the mean and variance of its trait distribution nor go to the opposite extreme of tracking the entire discretized distribution (i.e., a discretized full model). They combine a multi-species model with an aggregate approach and split the community into a limited number of entities such as species or functional groups. The adjustment of their mean trait values and variances to ambient conditions within a limited trait range can then be described more adequately by the aggregate model approach (Norberg et al. 2012; Klauschies et al. 2016). For example, the phytoplankton community can be separated into two functional groups

(e.g., edible and less edible algae) at the trait value of the turning point of the logistic function. This results in two only weakly non-linear fitness functions for each group covering more restricted trait ranges with smaller variance where $\bar{x}$ better represents the properties of the functional group. Such an increase in food web resolution was advocated or used by Norberg et al. (2001) and Terseleer et al. (2014) to improve the accuracy of ecological models. A similar strategy is employed in some management models more strongly tailored to specific systems that split e.g., the phyto- or zooplankton community into 2 or more functional groups (Baretta et al. 1995; Prowe et al. 2014). Our results show that such an increase in model complexity and computational effort is warranted for the sake of the obtainable accuracy. Errors in the speed of biomass, trait, and variance dynamics may cause a temporal mismatch between abiotic forcing, community dynamics, and adjustment to altered conditions. Thus, evaluating the prevailing shape of the trait distributions, potentially subdividing the trait range into two or more groups (hybrid model), and employing a data-based moment closure should improve our skills to manage ecosystem appropriately.

To conclude, our newly developed classification scheme relying solely on skewness and kurtosis overcomes previous operational problems in comparing the shape of observed trait distributions. For freshwater phytoplankton they ranged from peaked to highly skewed and multi- or bimodal and mostly deviated substantially from normal distributions. The latter is to be expected if many of the trait distributions at a given time or location cover a substantial part of the entire feasible trait range which gives rise to tight correlations between skewness and mean trait, and kurtosis and variance. As this likely holds for many communities the common use of normal-based moment closures in aggregate models needs reconsideration. At the same time, these correlations enhance the performance of data-based moment closures. Accordingly, this approach yielded mostly reliable predictions for the biomass and trait changes at least for weakly non-linear fitness functions. Thus, we strongly recommend to use this method, if required combined with a hybrid model, when tailoring aggregate models to specific systems. However, predictions of the rate of change in the trait variance and even its direction were subject to substantial errors, which may hamper a realistic assessment of the maintenance of biodiversity, biomass-trait feedbacks, and eco-evolutionary cycles. For a moderately non-linear logistic fitness function, all aggregate models deviated often strongly from the true values for biomass, trait and variance dynamics which calls for combining the species sorting with the aggregate model approach. Overall, accounting in a fully quantitative way for the naturally inherent biodiversity and the resulting potential to adapt to ambient conditions remains a challenge for natural communities.

## References


Abrams, P. A., Y. Harada, and H. Matsuda. 1993. On the relationship between quantitative genetic and ESS models. Evolution **47**: 982–985. doi:10.1111/j.1558-5646.1993.tb01254.x

Acevedo-Trejos, E., G. Brandt, J. Bruggeman, and A. Merico. 2015. Mechanisms shaping size structure and functional diversity of phytoplankton communities in the ocean. Sci. Rep. **5**: 8918. doi:10.1038/srep08918

Akpalu, W. 2009. Economics of biodiversity and sustainable fisheries management. Ecol. Econ. **68**: 2729–2733. doi:10.1016/j.ecolecon.2009.05.014

Baretta, J. W., W. Ebenhöh, and P. Ruardij. 1995. The European Regional Seas Ecosystem model, a complex marine ecosystem model. Netherlands J. Sea Res. **33**: 23–246. doi:10.1016/0077-7579(95)90047-0

Blest, D. C. 2003. A new measure of kurtosis adjusted for skewness. Aust. N. Z. J. Stat. **45**: 175–179. doi:10.1111/1467-842X.00273

Bolnick, D. I., and others. 2011. Why intraspecific trait variation matters in community ecology. Trends Ecol. Evol. **26**: 183–192. doi:10.1016/j.tree.2011.01.009

Brandt, G., A. Merico, B. Vollan, and A. Schlüter. 2012. Human adaptive behavior in common pool resource systems. Plos One **7**: e52763. doi:10.1371/journal.pone.005276

Burns, C. W. 1968. The relationship between body size of filter-feeding Cladocera and the maximum size of particle ingested. Limnol. Oceanogr. **13**: 675–678. doi:10.4319/lo.1968.13.4.0675

Cortez, M. H. 2011. Comparing the qualitatively different effects rapidly evolving and rapidly induced defences have on predator-prey interactions. Ecol. Lett. **14**: 202–209. doi:10.1111/j.1461-0248.2010.01572.x

Coutinho, M. R., T. Klauschies, and U. Gaedke. 2016. Bimodal trait distributions with large variances question the reliability of trait-based aggregate models. Theor. Ecol. **9**: 389–408. doi:10.1007/s12080-016-0297-9

DeCarlo, L. T. 1997. On the meaning and use of kurtosis. Psychol. Methods **2**: 292–307. doi:10.1037/1082-989X.2.3.292

Dercole, F., R. Ferriere, A. Gragnani, and S. Rinaldi. 2006. Coevolution of slow-fast populations: Evolutionary sliding, evolutionary pseudo-equilibria and complex Red Queen dynamics. Proc. R. Soc. B Biol. Sci. **273**: 983–990. doi:10.1098/rspb.2005.3398

Dorić, D., E. Nikolić-Dorić, V. Jevremović, and J. Mališić. 2009. On measuring skewness and kurtosis. Qual. Quant. **43**: 481–493. doi:10.1007/s11135-007-9128-9

Downing, A. S., S. Hajdu, O. Hjerne, S. A. Otto, T. Blenckner, U. Larsson, and M. Winder. 2014. Zooming in on size distribution patterns underlying species coexistence in Baltic Sea phytoplankton. Ecol. Lett. **17**: 1219–1227. doi:10.1111/ele.12327

Ellner, S. P., and L. Becks. 2011. Rapid prey evolution and the dynamics of two-predator food webs. Theor. Ecol. **4**: 133–152. doi:10.1007/s12080-010-0096-7

Enquist, B. J., J. Norberg, S. P. Bonser, C. Violle, C. T. Webb, A. Henderson, L. L. Sloat, and V. M. Savage. 2015. Scaling from traits to ecosystems: Developing a general trait driver theory via integrating trait-based and metabolic scaling theories. Adv. Ecol. Res. **52**: 249–318. doi:10.1016/bs.aecr.2015.02.001

Gaedke, U. 1992. The size distribution of plankton biomass in a large lake and its seasonal variability. Limnol. Oceanogr. **37**: 1202–1220. doi:10.4319/lo.1992.37.6.1202

Gaedke, U. 1998. Functional and taxonomical properties of the phytoplankton community: Interannual variability and response to re-oligotrophication. Arch. Hydrobiol. Spec. Issues Advances in Limnology. **53**: 119–141.

Gandhi, A., S. Levin, and S. Orszag. 2000. Moment expansions in spatial ecological models and moment closure through Gaussian approximation. Bull. Math. Biol. **62**: 595–632. doi:10.1006/bulm.1999.0119

Griffiths, D. 1986. Size-abundances relations in communities. Am. Nat. **127**: 140–166. doi:10.1086/284475

Hillebrand, H., and B. Matthiessen. 2009. Biodiversity in a complex world: Consolidation and progress in functional biodiversity research. Ecol. Lett. **12**: 1405–1419. doi:10.1111/j.1461-0248.2009.01388.x

Horn, H. 2003. The relative importance of climate and nutrients in controlling phytoplankton growth in Saidenbach Reservoir. Hydrobiologia **504**: 159–166. doi:10.1023/B:HYDR.0000008515.38353.de

Horn, H., L. Paul, W. Horn, and T. Petzoldt. 2011. Long-term trends in the diatom composition of the spring bloom of a German reservoir: Is *Aulacoseira subarctica* favoured by warm winters? Freshw. Biol. **56**: 2483–2499. doi:10.1111/j.1365-2427.2011.02674.x

Horn, H., L. Paul, W. Horn, D. Uhlmann, and I. Röske. 2015. Climate change impeded the re-oligotrophication of the Saidenbach Reservoir. Int. Rev. Hydrobiol. **100**: 43–60. doi:10.1002/iroh.201401743

Jarque, C. M., and A. K. Bera. 1987. A test for normality of observations and regression residuals. Int. Stat. Rev. **55**: 163–172. doi:10.2307/1403192

Jones, M., J. Rosco, and A. Pewsey. 2011. Skewness-invariant measures of kurtosis. Am. Stat. **65**: 89–95. doi:10.1198/tast.2011.10194

Klaassen, C. A., P. J. Mokveld, and B. Van Es. 2000. Squared skewness minus kurtosis bounded by 186/125 for unimodal distributions. Stat. Probab. Lett. **50**: 131–135. doi:10.1016/S0167-7152(00)00090-0

Klauschies, T., D. Vasseur, and U. Gaedke. 2016. Trait adaptation promotes species coexistence in diverse predator and prey communities. Ecol. Evol. **6**: 4141–4159. doi:10.1002/ece3.2172

Kremer, C. T., and C. A. Klausmeier. 2013. Coexistence in a variable environment: Eco-evolutionary perspectives. J. Theor. Biol. **339**: 14–25. doi:10.1016/j.jtbi.2013.05.005

Lampert, W. 1978. A field study on the dependence of the fecundity of Daphnia spec. of food concentration. Oecologia **36**: 363–369. doi:10.1007/BF00348062

Lampert, W., and U. Sommer. 2007. Limnoecology. The ecology of lakes and rivers, 336 p. Oxford Univ. Press.

Lande, R. 1976. Natural-selection and random genetic drift in phenotypic evolution. Evolution **30**: 314–334. doi:10.1111/j.1558-5646.1976.tb00911.x

Lande, R. 1982. A quantitative genetic theory of life history evolution. Ecology **63**: 607–615. doi:10.2307/1936778

Litchman, E., C. A. Klausmeier, O. M. Schofield, and P. G. Falkowski. 2007. The role of functional traits and trade-offs in structuring phytoplankton communities: Scaling from cellular to ecosystem level. Ecol. Lett. **10**: 1170–1181. doi:10.1111/j.1461-0248.2007.01117.x

McGill, B. J., B. J. Enquist, E. Weiher, and M. Westoby. 2006. Rebuilding community ecology from functional traits. Trends Ecol. Evol. **21**: 178–185. doi:10.1016/j.tree.2006.02.002

Merico, A., J. Bruggeman, and K. Wirtz. 2009. A trait-based approach for downscaling complexity in plankton ecosystem models. Ecol. Modell. **220**: 3001–3010. doi:10.1016/j.ecolmodel.2009.05.005

Merico, A., G. Brandt, S. L. Smith, and M. Oliver. 2014. Sustaining diversity in trait-based models of phytoplankton communities. Front. Ecol. Evol. **2**: 1–8. doi:10.3389/fevo.2014.00059

Mougi, A. 2012. Unusual predator–prey dynamics under reciprocal phenotypic plasticity. J. Theor. Biol. **305**: 96–102. doi:10.1016/j.jtbi.2012.04.012

Norberg, J. 2004. Biodiversity and ecosystem functioning: A complex adaptive systems approach. Limnol. Oceanogr. **49**: 1269–1277. doi:10.4319/lo.2004.49.4_part_2.1269

Norberg, J., D. P. Swaney, J. Dushoff, J. Lin, R. Casagrandi, and S. A. Levin. 2001. Phenotypic diversity and ecosystem functioning in changing environments: A theoretical framework. Proc. Natl. Acad. Sci. USA **98**: 11376–11381. doi:10.1073/pnas.171315998

Norberg, J., M. C. Urban, M. Vellend, C. A. Klausmeier, and N. Loeuille. 2012. Eco-evolutionary responses of biodiversity to climate change. Nat. Clim. Chang. **2**: 747–751. doi:10.1038/nclimate1588

Pearson, K. 1929. Editorial note on inequalities for moments of frequency functions and for various statistical constants. Biometrika **21**: 370–375. doi:10.1093/biomet/21.1-4.361

Peters, R. H. 1983. The ecological implications of body size, 329 p. Cambridge Univ. Press.

Pfister, R., K. A. Schwarz, M. Janczyk, R. Dale, and J. B. Freeman. 2013. Good things peak in pairs: A note on the bimodality coefficient. Front. Psychol. **4**: 1–4. doi:10.3389/fpsyg.2013.00700

Prowe, A. E. F., M. Pahlow, S. Dutkiewicz, and A. Oschlies. 2014. How important is diversity for capturing environmental-change responses in ecosystem models? Biogeosciences **11**: 3397–3407. doi:10.5194/bg-11-3397-2014

Rocha, M. R., D. A. Vasseur, M. Hayn, M. Holschneider, and U. Gaedke. 2011*a*. Variability patterns differ between standing stock and process rates. Oikos **120**: 17–25. doi:10.1111/j.1600-0706.2010.18786.x

Rocha, M. R., U. Gaedke, and D. A. Vasseur. 2011*b*. Functionally similar species have similar dynamics. J. Ecol. **99**: 1453–1459. doi:10.1111/j.1365-2745.2011.01893.x

Rocha, M. R., D. A. Vasseur, and U. Gaedke. 2012. Seasonal variations alter the impact of functional traits on plankton dynamics. Plos One **7**: e51257. doi:10.1371/journal.pone.0051257

Saloniemi, I. 1993. A coevolutionary predator-prey model with quantitative characters. Am. Nat. **141**: 880–896. doi:10.1086/285514

Savage, V. M., C. T. Webb, and J. Norberg. 2007. A general multi-trait-based framework for studying the effects of biodiversity on ecosystem functioning. J. Theor. Biol. **247**: 213–229. doi:10.1016/j.jtbi.2007.03.007

Smith, S. L., S. M. Vallina, and A. Merico. 2016. Phytoplankton size-diversity mediates an emergent trade-off in ecosystem functioning for rare versus frequent disturbances. Sci. Rep. **6**: 34170. doi:10.1038/srep34170

Terseleer, N., J. Bruggeman, C. Lancelot, and N. Gypens. 2014. Trait-based representation of diatom functional diversity in a plankton functional type model of the eutrophied southern North Sea. Limnol. Oceanogr. **59**: 1958–1972. doi:10.4319/lo.2014.59.6.1958

Tirok, K., and U. Gaedke. 2007. The effect of irradiance, vertical mixing and temperature on spring phytoplankton dynamics under climate change: Long-term observations and model analysis. Oecologia **150**: 625–642. doi:10.1007/s00442-006-0547-4

Tirok, K., and U. Gaedke. 2010. Internally driven alternation of functional traits in a multispecies predator-prey system. Ecology **91**: 1748–1762. doi:10.1890/09-1052.1

Tirok, K., B. Bauer, K. Wirtz, and U. Gaedke. 2011. Predator-prey dynamics driven by feedback between functionally diverse trophic levels. Plos One **6**: e27357. doi:10.1371/journal.pone.0027357

Turelli, M., and N. H. Barton. 1994. Genetic and statistical analyses of strong selection on polygenic traits: What, me normal? Genetics **138**: 913–941.

Vasseur, D. A., and U. Gaedke. 2007. Spectral analysis unmasks synchronous and compensatory dynamics in plankton communities. Ecology **88**: 2058–2071. doi:10.1890/06-1899.1

Weithoff, G. 2003. The concepts of 'plant functional types' and 'functional diversity' in lake phytoplankton – a new understanding of phytoplankton ecology? Freshw. Biol. **48**: 1669–1675. doi:10.1046/j.1365-2427.2003.01116.x

Weithoff, G., M. Rocha, and U. Gaedke. 2015. Comparing seasonal dynamics of functional and taxonomic diversity reveals the driving forces underlying phytoplankton community structure. Freshw. Biol. **60**: 758–767. doi:10.1111/fwb.12527

Wirtz, K. W. 2013. Mechanistic origins of variability in phytoplankton dynamics. Part I: Niche formation revealed by a size-based model. Mar. Biol. **160**: 2319–2335. doi:10.1007/s00227-012-2163-7

Wirtz, K. W., and B. Eckhardt. 1996. Effective variables in ecosystem models with an application to phytoplankton succession. Ecol. Modell. **92**: 33–53. doi:10.1016/0304-3800(95)00196-4

Wirtz, K. W., and C. Lemmen. 2003. A global dynamic model for the neolithic transition. Clim. Change **59**: 333–367. doi:10.1023/A:1024858532005

Wirtz, K. W., and U. Sommer. 2013. Mechanistic origins of variability in phytoplankton dynamics. Part II: Analysis of mesocosm blooms under climate change scenarios. Mar. Biol. **160**: 2503–2516. doi:10.1007/s00227-013-2271-z

Wyszomirski, T. 1992. Detecting and displaying size bimodality: Kurtosis, skewness and bimodalizable distributions. J. Theor. Biol. **158**: 109–128. doi:10.1016/S0022-5193(05)80649-6

Zimmer, K. D., M. A. Hanson, M. G. Butler, and W. G. Duffy. 2001. Size distribution of aquatic invertebrates in two prairie wetlands, with and without fish, with implications for community production. Freshw. Biol. **46**: 1373–1386. doi:10.1046/j.1365-2427.2001.00759.x

## Acknowledgments

We thank Moritz Bach, Annika Busse, Ralf Hofmann, and René Sachse who contributed to the data analysis and greatly appreciate the comments by Ruben Ceulemans, Christian Guill and Ellen van Velzen on previous versions of the manuscript. We are very grateful to Heidemarie Horn who provided the phytoplankton data from Saidenbach Reservoir. She was funded by the Academy of Science of Saxony, SAW, Germany. The German Research Foundation (DFG, GA 401/19-1 and Ga 401/26-1) funded Toni Klauschies.

## Conflict of Interest

None declared.

*Submitted 09 January 2017*
*Revised 25 July 2017*
*Accepted 13 September 2017*

*Associate editor: Paul Kemp*